Theory of resonant charge transfer in ion-surface collisions at grazing incidence at intermediate velocities

Joachim Burgdörfer

University of Tennessee, Knoxville, Tennessee 37996
and Oak Ridge National Laboratory, Oak Ridge, Tennessee 37831

Eckart Kupfer and Helmut Gabriel

Institut für Atom- und Festkörperphysik, Freie Universität Berlin, Arnimallee 14, Berlin 33, West Germany

We present a multichannel theory for resonant charge transfer in ion-surface collisions at grazing incidence at intermediate velocities ($v \cong 1$ a.u.) taking into account the nonorthogonality of the initial and the final states. Kinematic resonances occur between the atomic projectile levels and the Galilei-shifted conduction band of a metal. The time-dependent Schrödinger equation can be solved in the adiabatic approximation for the slow perpendicular motion ($v_{\perp} \ll 1$). As an application we calculate the complete $n = 2$ density matrix for H($n = 2$) following proton scattering at a gold surface at grazing incidence ($\theta = 5°$). The shape of the charge cloud around the receding hydrogen atom is determined.

I. INTRODUCTION

The experimental technique of inelastic ion-surface scattering at grazing incidence under small grazing angles $\theta \leq 5°$ has been recently successfully applied in a large number of investigations in different subfields. They include the study of the polarization characteristics of the excited atomic manifold formed during the collision process,[1-3] the production of nuclear-spin-polarized beams[4] surface channeling experiments for single-crystal targets,[5] and the detection of local and long-range magnetic order at surfaces.[6]

From the viewpoint of atomic collision theory, ion-surface scattering provides the opportunity to study collision dynamics under unusual circumstances. Inelastic processes are simultaneously governed by two different time (or velocity) scales: a fast motion of the projectile, $v_{\parallel} \cong |\mathbf{v}| \cong v_F$ (and v_0) in the surface plane and a slow adiabatic motion perpendicular to the surface, $v_{\perp} \ll (v_F, v_0)$. [The Fermi velocity v_F and the atomic orbital velocity v_0 (Bohr velocity) are the characteristic internal velocities of the transferred electron in its initial and final states.] A proper treatment requires, therefore, the combination of methods used in both high-energy and low-energy atomic collisions. Another interesting feature is the dominance of contributions from distant collisions since projectile ions specularly reflected at clean surfaces undergo an array of extremely soft collisions with the outermost atomic surface layer. The point of closest approach is determined by $v_{\perp}$.

Theoretical studies of the electron pickup in ion-surface collisions have been performed in the limit of slow collision velocities, $v \ll v_F, v_0$, using the fixed-ion approximation.[7-10] The transition rate is calculated at fixed ion-surface distances and then integrated over all distances to give the capture probability. This static probability model

does not provide accurate estimates for the relative phases of scattering amplitudes needed for the density matrix and cannot be applied to the present case of intermediate velocities. At high velocities $v \gg (v_F, v_0)$ the first-order (Born) approximation has been used[11,12] to calculate the density matrix for beam-tilted foil interaction as well as for ion-surface scattering. While good qualitative agreement with experimental data is found, a direct quantitative comparison is complicated by the fact that the use of a first-order approximation is conceptually not well founded.

More recently, a nonperturbative approach better suited for intermediate velocities using an Anderson model Hamiltonian[13,14] has been suggested. The difficulty with this approach is that it neglects the multichannel nature of the rearrangement process and its evaluation invokes rather restrictive model assumptions regarding the analytic structure of the coupling matrix elements.

The key point of the present treatment is that electron capture is an intrinsic multichannel process with asymptotic initial (ϕ_k) and final state (ϕ_j) belonging to different channel Hamiltonians. This requires the proper identification of relevant channel perturbations and the inclusion of effects due to the nonorthogonality[15] of the initial and the final states. At intermediate parallel velocities $v_{\parallel} \cong v_F$, charge transfer proceeds through a kinematic resonance. The effect of the relative motion is to bring about degeneracies between discrete atomic levels and the Galilei-shifted occupied conduction-band levels[13,16] as seen in the projectile frame (Fig. 1). While at $v_{\parallel} \ll v_F$ the atomic spectrum taken to be hydrogenic in the following is nondegenerate with occupied levels, at velocities $v \cong v_{\parallel} \cong v_F$ excited states are in resonance simultaneously with portions of the occupied as well as empty levels of the Galilei-shifted band structure. A continual creation of excited states by resonant capture and subsequent destruc-
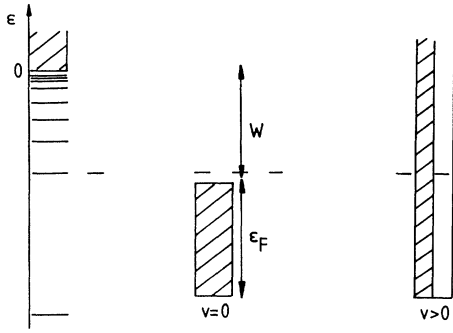
FIG. 1. Kinematic resonance as seen in the projectile frame, schematically. At $v=0$ occupied levels (shaded area) are nondegenerate with atomic spectrum (ε_F: Fermi energy; W is the work function). At intermediate velocities atomic levels are in resonance with both occupied and empty levels of the Galilei-shifted band structure.

tion by resonant ionization is expected to be the dominant mode of formation.

The plane of the paper is as follows. The general multichannel kinematic resonance scattering (KRS) theory is outlined in Sec. II. In Sec. III we briefly review the density-matrix description of excited hydrogenic manifolds. In Sec. IV we apply the KRS theory to the formation of the H($n=2$) manifold following proton scattering at a gold surface. The Au surface will be treated in the nearly-free-electron (jellium) approximation. The complete $n=2$ density matrix will be calculated and the effects of incoherent (nonresonant) loss processes due to electron-electron scattering will be analyzed. The relation between the present KRS description to other theories is outlined in Sec. V. Concluding remarks are given in Sec. VI. Atomic units are used throughout unless otherwise noted.

II. THEORY OF KINEMATIC RESONANCE SCATTERING

We are concerned with charge transfer through a kinematic resonance in a grazing-incidence collision. While the resonant transfer (a time-dependent tunneling process) between the atomic level and the conduction band is expected to dominate at intermediate velocities $v \simeq v_F$, other mechanisms to create excited states may be simultaneously present and will eventually dominate at higher velocities. They include direct capture from inner shells of the target as well as two-step processes of capture into the ground state followed by excitation. Those processes resembling binary ion-atom collisions become important when projectile levels come into resonance with inner shells of the target at higher speeds. We will neglect those processes from the onset. As we will discuss below, its justification requires a detailed analysis on a case-by-case basis.

We treat the transfer problem in an independent-particle model (IPM) neglecting correlation effects. This is justified for single-electron capture while the H$^-$ for-

mation by double capture requires a more sophisticated approach. We furthermore assume an ideal structureless surface with planar translation symmetry. The motion of the proton can be quite accurately approximated by a classical trajectory since the de Broglie wavelength λ_d is small compared to characteristic distances in the target or projectile. We will in the following focus only on the outgoing portion of the trajectory of the reflected proton which is approximated by a constant-velocity straight line.

We adopt the projectile frame as the frame of reference with the proton located at the origin. Accordingly, the jellium surface has the velocity

$$\mathbf{v}_T = -\hat{\mathbf{x}} v_{\parallel} - \hat{\mathbf{z}} v_{\perp} \ . \tag{1}$$

The distance of the surface from the proton is given by

$$R(t) = R_0 + v_{\perp} t \ , \tag{2}$$

where the initial distance from the surface at $t=0$ is denoted by R_0. We will later analyze the influence of the cutoff parameter R_0. The angle between $\mathbf{v}$ and the surface plane is $\theta \leq 5°$. Equation (2) clearly becomes invalid near the point of closest approach (of the order of $R \leq 1$ a.u.) or for the incoming part of the trajectory. As we will show below this part of the trajectory will not effectively contribute to the formation of the final electronic state because of the continual destruction of excited states in the immediate vicinity of the surface.

Using a classically prescribed trajectory, the electronic Hamiltonian becomes time dependent. It can be decomposed as

$$H = H_i + V_i = H_f + V_f \ , \tag{3}$$

where $H_{i(f)}$ denotes the entrance (exit) channel Hamiltonian and $V_{i(f)}$ is the corresponding channel perturbation. The asymptotic initial states of the conduction electron, $\phi_{\mathbf{k}}$, and final atomic orbitals, ϕ_j, are eigenstates of the channel Hamiltonians H_i and H_f, respectively. In the numerical calculation of Sec. IV we will choose the Sommerfeld model for the semi-infinite electron gas,

$$H_i = H_0 + V_J \ , \tag{4a}$$

where H_0 is the electronic kinetic energy and V_J is the jellium potential

$$V_J = -V_0 \Theta(-z - R(t)) \ , \tag{4b}$$

with V_0 the energy of the bottom of the conduction band and Θ the unit step function. The exit-channel Hamiltonian is taken to be hydrogenic,

$$H_f = H_0 + V_C \ , \tag{5}$$

where the electron-proton Coulomb interaction is denoted by

$$V_C = -1/r \ . \tag{6}$$

As the entrance channel perturbation we take

$$V_i = V_C + (V_C^I + V_e^I)\Theta(z + R(t)) \ , \tag{7}$$

where V_C^I and V_e^I denote the interactions with the proton image charge and with the electronic self-image charge.

The image potentials describe the collective response of the electron gas to lowest order within the IPM. The use of classical image potential is justified[17] for distances larger than the surface plasmon screening length $\lambda_s = v/\omega_s$ (ω_s is the surface plasmon frequency). The self-image potential V_e^I may also be included in H_i. However, analytic solutions for channel functions are available only in the asymptotic region ($z \to \infty$) (Ref. 14) which are inaccurate in the region of strong overlap. We therefore use for simplicity the Sommerfeld-model wave function for the electron gas.[8]

In the IPM for charge transfer, the exact wave function can be expanded in an overcomplete basis as

$$\psi(t) = \sum_j a_j(t)\phi_j + \sum_\mathbf{k} b_\mathbf{k}(t)\phi_\mathbf{k}(t) . \tag{8}$$

We use periodic boundary conditions for the metal wave function $\phi_\mathbf{k}$ in a quantization volume $\mathscr{V}$. As usual, we will eventually convert the sum over all discrete $\mathbf{k}$ values into an integral. Because of the fast parallel motion of the solid relative to the atom, the orbitals $\phi_\mathbf{k}$ have to be properly Galilei transformed by the use of translation factors[18] well known from high-energy ion-atom collisions. For a target with perfect translation symmetry where $\mathbf{k}_{||}$ is a good quantum number, this corresponds to displacement in momentum space by the momentum $-\mathbf{v}_{||}$,

$$\phi_{\mathbf{k}-\mathbf{v}_{||}}(\mathbf{r}+R(t)\hat{\mathbf{z}},t)=\phi_\mathbf{k}(\mathbf{r}+R(t)\hat{\mathbf{z}}+\mathbf{v}_{||}t,t)$$

$$\times \exp(-i\mathbf{v}_{||}\cdot\mathbf{r}_{||}-iv_{||}^2 t/2) . \tag{9}$$

In the Sommerfeld model we have

$$\phi_\mathbf{k}(\mathbf{r},t) = \frac{1}{\sqrt{\mathscr{V}}} e^{i\mathbf{k}_{||}\cdot\mathbf{r}_{||}} g(r_\perp) e^{-i\varepsilon_\mathbf{k} t} , \tag{10}$$

with

$$g(r_\perp) = \left[e^{ik_z r_\perp} + \frac{ik_z+\delta}{ik_z-\delta} e^{-ik_z r_\perp} \right]\Theta(-r_\perp)$$

$$+ \frac{2ik_z}{ik_z-\delta} e^{-i\delta r_\perp}\Theta(r_\perp) \tag{11}$$

and

$$\varepsilon_\mathbf{k} = \tfrac{1}{2}k^2 - V_0 , \tag{12}$$

$$\delta = (2V_0 - k^2)^{1/2} . \tag{13}$$

We derive in the following a general expression for the amplitude for resonant charge transfer within the framework of the KRS theory. It is independent of the particular choice for the channel potentials [Eqs. (4)—(7)] and the target wave function [Eq. (10)]. It is only based on three essential assumptions: the independent-particle model, the perfect planar symmetry of the surface, and the adiabatic approximation for the perpendicular motion.

The Schrödinger equation with the Hamiltonian [Eq. (3)] can be converted to a coupled system of equations of motion for the amplitudes $a_j(t)$ and $b_\mathbf{k}(t)$. Restricting the expansion [Eq. (8)] to an atomic subspace of dimension N, we find for the vector of amplitudes

$$A(t) = (a_j(t))_{1 \leq j \leq N} \tag{14}$$

the set of equations

$$\underline{H}A(t) = \sum_\mathbf{k} M(\mathbf{k})b_\mathbf{k}(t) \tag{15a}$$

and

$$\left[i\frac{d}{dt} - \bar{\varepsilon}_\mathbf{k} \right]b_\mathbf{k}(t) = M^\dagger(\mathbf{k})\cdot A(t) . \tag{15b}$$

In (15), the elements of the matrix $\underline{H}$ in the atomic state space are given by

$$H_{j,j'} = \left[i\frac{d}{dt} - \varepsilon_j \right]\delta_{j,j'} - \langle \phi_j | V_f | \phi_{j'} \rangle , \tag{16}$$

and the vectors of coupling matrix element are given by

$$M_j(\mathbf{k}) = N_j \left[\varepsilon_\mathbf{k} - i\frac{d}{dt} \right] + \langle \phi_j | V_i | \phi_\mathbf{k} \rangle , \tag{17a}$$

$$M_j^\dagger(\mathbf{k}) = N_j^* \left[\varepsilon_\mathbf{k} - i\frac{d}{dt} \right] + \langle \phi_\mathbf{k} | V_i | \phi_j \rangle . \tag{17b}$$

Furthermore, the right-hand side of Eq. (15b) denotes a scalar product in the N-dimensional atomic-state space. The elements of the vector of overlap matrix elements are denoted by

$$N_j = \langle \phi_j | \phi_\mathbf{k} \rangle , \tag{18}$$

and

$$\bar{\varepsilon}_\mathbf{k} = \varepsilon_\mathbf{k} + \langle \phi_\mathbf{k} | V_i | \phi_\mathbf{k} \rangle \tag{19}$$

defines the perturbed conduction-band energies including the entrance-channel distortion.

The system of coupled equations can now be solved in the adiabatic approximation exploiting the fact that $v_\perp \ll 1$ for grazing-incidence collisions. We first solve Eq. (15) in the limit $v_\perp = 0$ [i.e., exact parallel motion with $R(t) = R_0$] for finite time intervals $(0,t)$. In a subsequent step we treat the implicit time dependence due to the $R(t)$ dependence of the coupling matrix elements in the adiabatic approximation. This allows the extraction of scattering amplitudes as a convergent limit $a_j(t \to \infty)$.

In the first step we employ the Laplace transform

$$\tilde{a}_j(s) = \int_0^\infty e^{-st} a_j(t)dt \tag{20}$$

leading to the system of equations

$$\underline{\tilde{H}}(s)\tilde{A}(s) = \sum_\mathbf{k} [\tilde{M}(\mathbf{k},s)\tilde{b}_\mathbf{k}(s) + i\Theta(k_f - |\mathbf{k}-\mathbf{v}_{||}|)N] , \tag{21a}$$

$$(is - \bar{\varepsilon}_\mathbf{k})\tilde{b}_\mathbf{k}(s) = \tilde{M}^\dagger(\mathbf{k},s)\cdot\tilde{A}(s) + i\Theta(k_f - |\mathbf{k}-\mathbf{v}_{||}|) . \tag{21b}$$

In Eq. (21) we have incorporated the initial conditions for charge transfer [$a_j(0)=0$, $b_\mathbf{k}(0)=\Theta(k_f - |\mathbf{k}-\mathbf{v}_{||}|)$]. The matrix $\underline{\tilde{H}}(s)$ and the vector $\tilde{M}(\mathbf{k},s)$ are defined in parallel with the corresponding quantities in t space. They are given by Eqs. (16) and (17) upon replacing d/dt by the Laplace variable s.

Inserting now Eq. (21b) in (21a) and specializing to the

case of a degenerate subspace with unperturbed atomic energy ε_a, one finds after some straightforward algebra the subspace matrix equation

$$[(is - \varepsilon_a)\underline{1} - \underline{\Sigma}(s)]\tilde{A}(s) = i \sum_{\substack{\mathbf{k} \\ (|\mathbf{k} - \mathbf{v}_\parallel| \leq k_f)}} \frac{\tilde{M}(\mathbf{k}, -i\bar{\varepsilon}_\mathbf{k})}{is - \bar{\varepsilon}_\mathbf{k}} .$$

(22)

The matrix elements $\Sigma_{j,j'}(s)$ of the self-energy matrix for the atomic manifold are given by

$$\Sigma_{j,j'}(s) = \langle \phi_j | V_f | \phi_{j'} \rangle + \sum_\mathbf{k} \frac{\tilde{M}_j(\mathbf{k}, s)\tilde{M}^\dagger_{j'}(\mathbf{k}, s)}{is - \bar{\varepsilon}_\mathbf{k}} .$$

(23)

The complex self-energies $\Sigma_j = is_j$ $(1 \leq j \leq N)$ are determined by the eigenvalue equation

$$\det[is\underline{1} - \underline{\Sigma}(s)] = 0 .$$

(24)

We use a single label j for the eigenvalues in order to distinguish them from the diagonal elements of $\underline{\Sigma}$ in the original basis. As usual, the real part Σ'_j describes the

shift of the energy level, while the imaginary part Σ''_j accounts for level broadening (damping) due to the presence of open decay channels into the solid. Note that in Eq. (23), the $\mathbf{k}$ sum (or, in the following, the $\mathbf{k}$ integral) extends over all $\mathbf{k}$, while in Eq. (22) only occupied states are included. We arrive here at a conceptual difficulty associated with the IPM. The state label $\mathbf{k}$ labels simultaneously a basis set employed in the equation of perturbed one-electron states as well as occupation numbers of an N-particle system. The sum in Eq. (23) includes therefore exclusion-principle-violating intermediate states. We will in the following distinguish between contributions to $\underline{\Sigma}'$ and to $\underline{\Sigma}''$ due to states $\mathbf{k}$ representing occupied orbitals. In the calculation of $\underline{\Sigma}'$ we will include exclusion-principle-violating (EPV) intermediate states similar to those in atomic many-body perturbation theory,[19] while we exclude all occupied $\mathbf{k}$ states in the calculation of $\underline{\Sigma}''$ since they correspond to closed channels for on-shell transitions into the solid. We will return to this point in Sec. IV.

Upon diagonalization, the inverse Laplace transform can be performed to give the new amplitude vector $C(t)$ with components

$$c_j(t) = -i \sum_{\substack{\mathbf{k} \\ (|\mathbf{k} - \mathbf{v}_\parallel| \leq k_f)}} \int_0^t dt' B_j(\mathbf{k}, -i\bar{\varepsilon}_\mathbf{k}) \exp\left[i \int_0^{t'} dt'' \bar{\varepsilon}_\mathbf{k} - i \int_{t'}^t dt''(\varepsilon_a + \Sigma_j)\right] .$$

(25)

The new coupling vector B is related to the original vector $\tilde{M}$, through

$$B = \underline{U}^{-1}\tilde{M} ,$$

(26)

where $\underline{U}$ is the matrix of eigenvectors of $\underline{\Sigma}$. The distance-dependent (or in the adiabatic approximation time-dependent) transformation matrix $\underline{U}$ is nonunitary since the coupling between the atomic system and the solid does not preserve unitarity within the atomic subspace. Similarly, the vector of new state amplitudes, $C = (c_j)_{1 \leq j \leq N}$, is related to the vector of unperturbed atomic amplitudes, $A = (a_j)_{1 \leq j \leq N}$, by

$$C = \underline{U}^{-1}A .$$

(27)

The amplitudes c_j describe the population amplitudes of strongly perturbed atomic states $\bar{\phi}_j$ in the vicinity of the surface. These perturbed states are eigenstates of $\underline{\Sigma}$.

Equation (25) is now well suited for the application of the adiabatic approximation in a second step. Accordingly, the integrands in the time integrals in Eq. (25) are treated as time dependent due to the $R(t)$ dependence of all matrix elements [e.g., $\underline{\Sigma}(t)$]. Furthermore, for nondegenerate states, the asymptotic scattering amplitudes are given in the adiabatic approximation by

$$\lim_{t \to \infty} a_j(t) = \lim_{t \to \infty} c_j(t) ,$$

(28)

where the correlation between a_j and c_j is determined by the nonintersecting ("adiabatic") self-energy curves Σ_j. For an asymptotically degenerate subspace and persistent

state mixture due to long-range couplings, Eq. (28) has to be modified. The inverse transformation

$$\lim_{t \to \infty} A(t) = \lim_{t \to \infty} \underline{U}(t)C(t)$$

(29)

should be used in this case with $\underline{U}$ restricted to the subspace under consideration. In our numerical study (Sec. IV) we will calculate (29) at a time t corresponding to a distance of 40 a.u. from the surface where the amplitudes as well as the transformation matrix $\underline{U}$ have approximately converged to their respective asymptotic values. Since we calculate the evolution only for $R(t) \geq R_0$, the scattering amplitudes [Eqs. (28) and (29)] depend on R_0. We will later show that they become practically independent of the cutoff parameter for sufficiently small R_0.

Due to the axial symmetry of atom-surface interaction with respect to the surface normal, self-energies belonging to states with identical magnetic qantum number m display level repulsion. In addition, if the diagonal elements of the original $\underline{\Sigma}$ matrix (the "diabatic" potential curves) belonging to states of the same representation of the $C_{\infty v}$ symmetry group cross each other, avoided crossings occur. This may lead to strong local dynamical couplings between different adiabatic potential curves. The validity of the adiabatic approximation requires in this case

$$\left| v_\perp \left\langle \bar{\phi}_j \left| \frac{d}{dR} \right| \bar{\phi}_{j'} \right\rangle \right| \ll |\Sigma'_j - \Sigma'_{j'}|$$

(30)

near the crossing point. A crude estimate on the effect of

nonadiabaticity can be given by replacing the adiabatic transformation [Eqs. (28) and (29)] by the corresponding sudden (diabatic) transformation, i.e., by using the transformation (29) at t values corresponding to the crossing point. The present formulation allows the calculation of the dynamical process of resonant charge transfer between atomic levels and the solid for a broad class of input matrix elements characterizing the static structure of the atom and of the surface at various levels of sophistication with a realistic amount of CPU time. For analytically or numerically known input parameters the determination of density matrix elements [see Eq. (31) below] requires a five-dimensional integration.

An appealing feature is that the present treatment takes into account coupling to all orders within a given subspace as well as nonorthogonality corrections.

III. THE DENSITY MATRIX

The maximum information available on the final atomic state formed in ion-surface collisions is contained in the atomic density matrix ρ. In terms of the scattering amplitudes a_j the density matrix is given by

$$\rho_{j,j'}(R_0) = \langle a_j a_{j'}^* \rangle , \tag{31}$$

where the angular brackets refer to an ensemble average (i.e., a partial trace) over unresolved observables such as the final state of the target, electronic and nuclear spin degrees of freedom, etc. In particular, since the hole state of the conduction band created by the electron transfer is not detected, the ensemble average includes an incoherent sum over all $\mathbf{k}$, i.e., the double sum appearing in Eq. (31) after inserting Eq. (25) is reduced to a single sum (or integral) over all $\mathbf{k}$ values. For later reference we have in Eq. (31) explicitly displayed the dependence of ρ on the cutoff parameter R_0. The diagonal elements of ρ describe the usual substate cross sections. Off-diagonal elements are a measure of the coherence between substate amplitudes.

In the following, we will consider the hydrogen atom. We choose an orbital angular momentum representation [the state label j stands for (nlm)] since spin-dependent fine-structure effects can be safely neglected for light systems at intermediate velocities. We note in passing that for heavier systems with larger spin-orbit splittings and frequencies of the order of the inverse of the ion-surface interaction time spin-dependent multiple scattering effects become observable.[20] For hydrogen, the fine structure leads only to effective depolarization[21] of the emitted radiation due to averaging over quantum beat oscillations.

The hydrogenic density matrix for a given n manifold can be parametrized in terms of quantum mechanical expectation values of dynamical atomic observables such as the orbital angular momentum $\mathbf{L}$ and the Runge-Lenz vector[22]

$$\mathbf{A} = \frac{n}{Z_p} [\tfrac{1}{2}(\mathbf{p} \times \mathbf{L} - \mathbf{L} \times \mathbf{p}) - Z_p \mathbf{r}/r] , \tag{32}$$

where Z_p is the ionic charge of the projectile. This allows a meaningful physical interpretation and even an intuitive semiclassical visualization of coherences between quantum scattering amplitudes in terms of parameters for a classical orbit. For later reference we give all expectation values of rank-1 tensors in terms of the $n=2$ density matrix

$$\langle A_x \rangle = \mathrm{Tr}(\rho A_x)/\mathrm{Tr}\rho = -2\sqrt{2}\,\mathrm{Re}(\rho_{200,211})/\mathrm{Tr}\rho , \tag{33a}$$

$$\langle A_z \rangle = 2\,\mathrm{Re}(\rho_{200,210})/\mathrm{Tr}\rho , \tag{33b}$$

$$\langle (\mathbf{L} \times \mathbf{A})_x \rangle = 2\sqrt{2}\,\mathrm{Im}(\rho_{200,211})/\mathrm{Tr}\rho , \tag{33c}$$

$$\langle (\mathbf{L} \times \mathbf{A})_z \rangle = -2\,\mathrm{Im}(\rho_{200,211})/\mathrm{Tr}\rho , \tag{33d}$$

$$\langle L_y \rangle = -2\sqrt{2}\,\mathrm{Im}(\rho_{211,210})/\mathrm{Tr}\rho . \tag{33e}$$

Note that the y component of the polar vectors $\mathbf{A}$ and $\mathbf{L} \times \mathbf{A}$ as well as the x and z components of the axial vector $\mathbf{L}$ vanish because of the reflection symmetry with respect to the x-z plane. Classically, $\mathbf{A}$ characterizes the orientation of the major axis of the Kepler ellipse. The magnitude $|\mathbf{A}|$ is proportional to the eccentricity of the orbit, or equivalently, to the dipole moment of the charge cloud. The expectation value $\langle L_y \rangle$ gives the atomic orientation (circulation) of the electron. The vector $\mathbf{L} \times \mathbf{A}$ points along the direction of the orbital velocity vector at the perihelion.

In addition, the density matrix can be related to the three normalized Stokes parameters S/I, M/I, and C/I, which characterize the polarization state of elliptically polarized light emitted in radiative decay following anisotropic (e.g., collisional) excitation. For a doublet $(^2P$-$^2S)$ transition and photon emission in the y direction, the Stokes parameters are given by[23]

$$\frac{S}{I} = \frac{14\sqrt{2}\,\mathrm{Im}\rho_{11,10}}{7\rho_{10,10} + 11\rho_{11,11} - 3\rho_{11,1-1}} , \tag{34a}$$

$$\frac{M}{I} = \frac{3(\rho_{10,10} - \rho_{11,11} + \rho_{11,1-1})}{7\rho_{10,10} + 11\rho_{11,11} - 3\rho_{11,1-1}} , \tag{34b}$$

$$\frac{C}{I} = \frac{-6\sqrt{2}\,\mathrm{Re}\rho_{11,10}}{7\rho_{10,10} + 11\rho_{11,11} - 3\rho_{11,1-1}} , \tag{34c}$$

where we have suppressed the principal quantum number in the state label. In (34) we have included the depolarization factors due to the fine structure but have neglected small additional depolarization effects caused by the hyperfine structure. The meaning of the relative Stokes parameters is as follows: S/I is roughly proportional to $\langle -L_y \rangle$, the atomic orientation [see Eq. (33e)], and gives the circular polarization; the Stokes parameters M/I and C/I give the linear polarization (i.e., the quadrupole deformation of the charge cloud) relative to the quantization axis and relative to the 45° line in the x-z plane, respectively. The experimental Stokes parameter M/I and C/I are often defined relative to the beam ($\hat{v}$) axis rather than relative to the surface normal ($\hat{z}$) (see also Figs. 12 and 14). In this case, Eqs. (34b) and (34c) have to be transformed according to standard rotation formulas for rank-2 tensors.

We note that the experimental observation of the coherence parameters of mixed parity [Eqs. (33a)–(33d)] requires the perturbation of the excited states by external electric fields.[24]

IV. NUMERICAL RESULTS

In this section we discuss the first numerical application of the KRS theory to the $n=2$ density matrix in hydrogen following grazing-incidence scattering ($\theta=5°$) of protons at a gold surface. In addition to the Sommerfeld model for the target Hamiltonian (Eq. 4) we will invoke a few more "technical" approximations in order to keep the numerics at a reasonable level of complexity. The latter seems to be appropriate in view of the overall simplicity of the description of the static structure of the target.

A. The Wigner-Weisskopf approximation

The most restrictive approximation we use is the Wigner-Weisskopf[25] (WW) approximation to the self-

energy matrix in analogy with the standard treatment of radiative decay. The error introduced by the WW approximation is largest for strong coupling between the atomic levels and the solid, i.e., at small distances $R \ll \langle r \rangle_n$. However, this region does not effectively contribute to the formation of atomic states as we will show below. In the WW approximation, the position of the pole in the self-energy matrix is approximated by its unperturbed value, i.e.,

$$\underline{\Sigma}(s) \cong \underline{\Sigma}(-i(\varepsilon_a+i\eta)) \ , \tag{35}$$

with $\eta=0^+$. The self-energy matrix Eq. (23) becomes now with the help of a standard distribution identity

$$\Sigma_{j,j'}(-i\varepsilon_a) = \langle \phi_j \mid V_f \mid \phi_{j'} \rangle + PP \sum_{\mathbf{k}} \frac{\widetilde{M}_j(\mathbf{k},-i\varepsilon_a)\widetilde{M}^{\dagger}_{j'}(\mathbf{k},-i\varepsilon_a)}{\varepsilon_a-\overline{\varepsilon}_{\mathbf{k}}} - i\pi \sum_{\mathbf{k}} \widetilde{M}_j(\mathbf{k},-i\varepsilon_a)\widetilde{M}^{\dagger}_{j'}(\mathbf{k},-i\varepsilon_a)\delta(\varepsilon_a-\overline{\varepsilon}_{\mathbf{k}}) \ . \tag{36}$$

In Appendix A we show that for Sommerfeld model wave function in the limit of complete delocalization (i.e., box volume $V \to \infty$),

$$\overline{\varepsilon}_{\mathbf{k}}=\varepsilon_{\mathbf{k}} \ , \tag{37}$$

i.e., the initial-channel distortion is negligible. We note that Eq. (37) does not hold in general for localized target states. Using (37) and the channel decomposition of H [Eq. (3)], Eq. (36) can be rewritten as

$$\Sigma_{j,j'}(-i\varepsilon_a) = \langle \phi_j \mid V_f \mid \phi_{j'} \rangle + PP\frac{\mathscr{V}}{(2\pi)^3}\int d^3\mathbf{k}\frac{\mid\langle \phi_j \mid V_f \mid \phi_{\mathbf{k}} \rangle\mid^2}{\varepsilon_a-\varepsilon_{\mathbf{k}}} - \pi i\frac{\mathscr{V}}{(2\pi)^3}\int d^3\mathbf{k}\mid\langle \phi_j \mid V_i \mid \phi_{\mathbf{k}} \rangle\mid^2\delta(\varepsilon_a-\varepsilon_{\mathbf{k}}) \ . \tag{38}$$

Equation (38) displays explicitly the importance of multichannel effects in the rearrangement process: In WW approximation the energy shift due to virtual transitions into off-shell intermediate states (the PP integral) and the damping term (containing the energy conserving δ function) are determined by different channel potentials. If one neglects the orthogonality correction from the onset as it is the case in a single-channel model, the entrance-channel potential V_i would also determine the energy shift yielding an unphysical nonzero value in the asymptotic limit $R \to \infty$. The latter follows from the fact that the overlap $\langle \phi_{\mathbf{k}} \mid \phi_j \rangle$ does not vanish in the limit $R \to \infty$ for states $\phi_{\mathbf{k}}$ belonging to the positive-energy continuum of the metal.

As discussed in Sec. II, the Pauli exclusion principle should be incorporated into the imaginary part of the self-energy matrix in order to remove spurious lifetime effects due to closed decay channels. In the WW approximation [Eq. (38)], this can be easily accomplished by redefining

$$\Sigma''_{j,j'}(-i\varepsilon_a) = \frac{-\pi\mathscr{V}}{(2\pi)^3}\int d^3\mathbf{k}\mid\langle \phi_j \mid V_i \mid \phi_{\mathbf{k}} \rangle\mid^2\delta(\varepsilon_a-\varepsilon_{\mathbf{k}})$$
$$\times[1-f(\mathbf{k}-\mathbf{v}_{\parallel},T)] \ , \tag{39}$$

where $f(\mathbf{k},T)$ is the Fermi distribution function at tem-

perature T (to be set $T=0$ in the following).

In addition to the WW approximation, we use the following approximation in evaluating the channel-potential matrix elements: We neglect the image potentials in the "two-center" matrix elements ($\sim \langle \phi_j \mid V_i \mid \phi_{\mathbf{k}} \rangle$) since they are defined only outside the surface where the matrix elements decay exponentially [note that $\varepsilon_{\mathbf{k}}<0$ in Eq. (39)]. On the other hand, the "one-center" matrix elements ($\sim \langle \phi_j \mid V_f \mid \phi_{j'} \rangle$) as well as the two-center matrix element ($\sim \langle \phi_j \mid V_f \mid \phi_{\mathbf{k}} \rangle$) in Eq. (38) are of long range. The latter follows from the fact that for off-shell energy values $\varepsilon_{\mathbf{k}}>0$ in the second term of Eq. (38), the target wave function is no longer exponentially damped. For these matrix elements we use a multipole expansion [Appendix B, Eq. (B2)] retaining all terms up to the order R^{-3}.

B. Self-energy matrix

The diagonal elements of the self-energy matrix [Eq. (23)] prior to the diagonalization play the role of "diabatic" complex potential curves. The real part $\Sigma'_{j,j}$ is displayed for the $n=2$ manifold in Fig. 2. We do not find level crossings near the surface ($1 \leq R \leq 40$ a.u.). Note, however, that at asymptotically large distances ($R \geq 10^2$ a.u.) crossings will occur when small interatomic interactions (Lamb shift, fine structure) equal the perturbations due to the surface. These crossings will be considered as
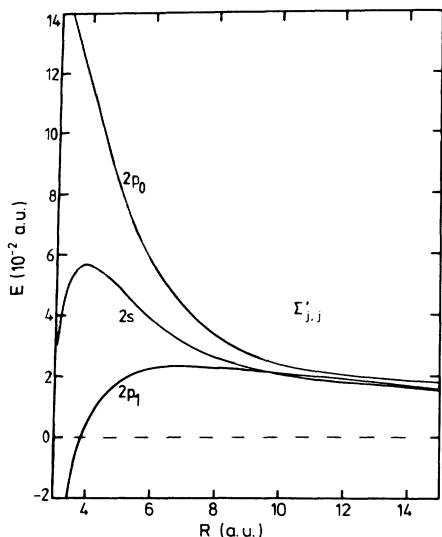
FIG. 2. Real part of the diagonal elements of the self-energy matrix, $\Sigma_{j,j'}$, as a function of the distance R from the jellium surface. Quantization axis is along the surface normal.

diabatic (i.e., nonavoided).

It is instructive to analyze the distinct physical contributions contained in the diabatic potential curves as shown in Fig. 3 for the $2p\pm1$ state. At large distances ($R \geq 10$ a.u.), the monopole term of the image potential [Eq. (B2)] dominates. For neutral atoms the dipole term vanishes while the quadrupole term ($\sim R^{-3}$) leads to a significant state-dependent modification of the R^{-1} term at distances $R \geq \langle r \rangle_n$. State-dependent shifts will play an important role for the phases of off-diagonal elements of the density matrix. We note that for $R \ll \langle r \rangle_n$, the multipole expansion, as well as for $R \leq \lambda_s$ the concept of a
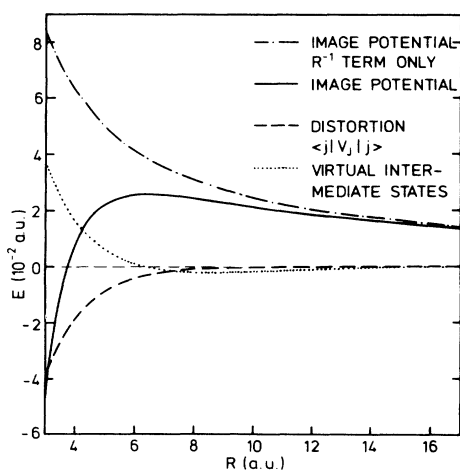
classical image potential ceases to be valid. At intermediate distances, exit-channel distortion effects due to the partial penetration of the atomic charge cloud into the solid ($\sim \langle \phi_j \mid V_J \mid \phi_j \rangle$) become important. They are of the same order of magnitude as image charge effects and give rise to additional state-dependent contributions. Finally, the energy shift due to virtual transitions into intermediate states (somewhat analogous to the Lamb shift) provides the dominant contribution at small distances and goes to zero like R^{-2} in the limit $R \to \infty$ as expected. We note this is only the case when the appropriate orthogonality correction is used. Within a single-channel theory neglecting N_j, this term approaches a finite value at asymptotic distances due to spurious overlap contributions.

Turning now to imaginary parts, the damping constants $\Sigma_{j,j}''$ (Fig. 4), we observe dramatic deviations from the mono-exponential decay frequently used in analytically solvable models. The pronounced local minimum for $-\Sigma_{2s,2s}''$ is caused by the radial node of the $2s$ wave function. Due to the exclusion principle correction to Σ'' [Eq. (39)], the damping constants become velocity dependent. In the velocity range under consideration ($v \sim 1$ a.u.) these corrections are smaller than 10% and can be neglected. We note, however, that the corrections can become more pronounced for lower velocities and lower-lying states where the Pauli principle severely restricts the number of open decay channels in a kinematic resonance.

The real part, $\Sigma_{2s,2p_0}'$, and the imaginary part, $\Sigma_{2s,2p_0}''$, of the only nonvanishing off-diagonal element of $\underline{\Sigma}$ are shown in Fig. 5. The magnitude of the real part is of the

FIG. 3. Contributions to the diagonal element of the self-energy matrix, $\Sigma_{2p_1,2p_1}'$: —·—·—·, monopole part of image potential; ———, image potential to order R^{-3}; — — —, distortion $\langle \phi_j \mid V_j \mid \phi_j \rangle$; and · · · ·, contributions from virtual intermediate states.
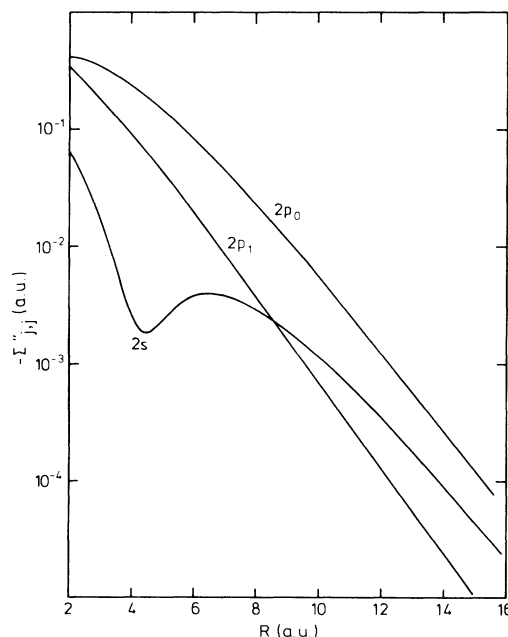

FIG. 4. Negative imaginary part (half of the damping constant) of the diagonal elements of the self-energy matrix, $-\Sigma_{j,j}'' = \gamma_{j,j}/2$, as a function of the distance R from the jellium surface. The surface normal is the quantization axis.
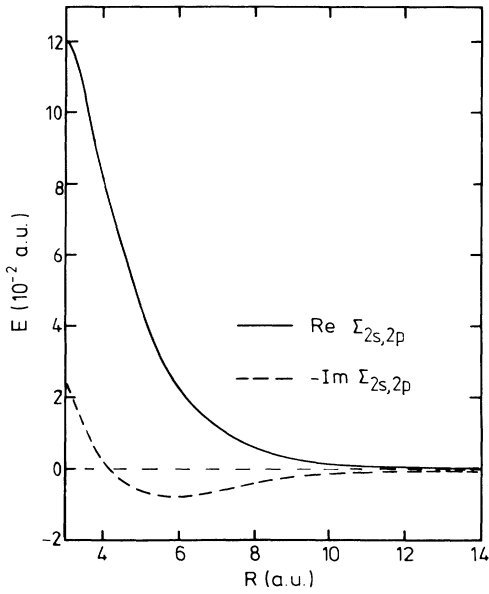
FIG. 5. Real and imaginary parts of the off-diagonal element of the self-energy matrix, $\Sigma_{2s,2p_0}$, as a function of the distance R from the jellium surface. The surface normal is the quantization axis.

same order of magnitude as the splitting between the diabatic energy curves for the $2s$ and the $2p_0$ state. This gives rise to a strong state mixture even at large distances from the surface. The off-diagonal elements decay asymptotically with the same power law (R^{-2}) as the diagonal elements. Thus the state mixture in degenerate manifolds persists as $R \rightarrow \infty$. The long-range $2s$-$2p_0$ coupling is due to the coupling to virtual intermediate states [the image potential part in V_f in the second term of Eq. (38)]. This long-range interaction is absent for neutral atoms if only the static image potential [the first term in Eq. (38)] is taken into account. In this latter case the $2s$-$2p_0$ coupling decays like R^{-4}.

Upon diagonalization of the self-energy matrix in the $(2s,2p_0)$ subspace, the complex adiabatic self-energies as a function of R can be found. The real parts, Σ'_j (Fig. 6), show the expected level repulsion while the pronounced minimum in the diabatic curve $\Sigma''_{2s,2s}$ is smeared out in the adiabatic curve due to the $2s$-$2p_0$ coupling (Fig. 7). Because of the absence of level crossings, the transformation matrix $\underline{U}$ is a slowly varying function of R as shown for the moduli of U_{11} and U_{12} in Fig. 8. The coefficients U_{11} and U_{12} give the admixture of the $2s$ and $2p_0$ states to the energetically lower-lying state $|\bar{\phi}_1\rangle$, which corresponds to a perturbed $2s$ state in the limit of weak coupling. A stronger variation has been observed for the phases in $\underline{U}$. We neglect the distance dependence of $\underline{U}$ in the following, using a constant matrix $[U(R=6 \text{ a.u.})]$ where capture is most likely to occur (see Fig. 9). The numerical values are found to be insensitive to variations of the value of R between $4 \leq R \leq 8$. Since the R dependence of $|\bar{\phi}_j\rangle$ is completely determined by matrix elements $U_{jj'}$, the adiabatic criterion [Eq. (30)] is approximately satisfied.
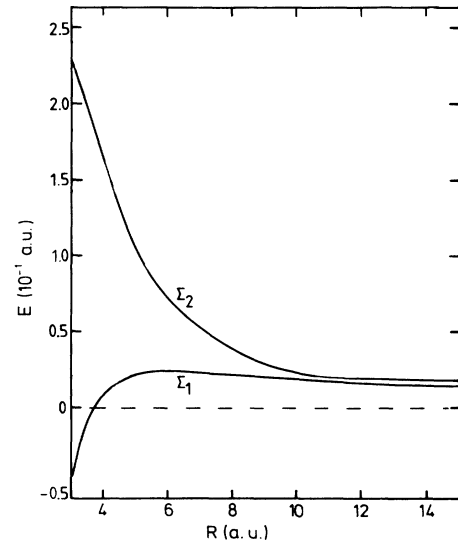
FIG. 6. Real part of the self-energies, $\Sigma'_j(j=1,2)$ ("adiabatic" potential curves) as a function of the distance a from the jellium surface. Note that adiabatic and diabatic are identical for the states $2p \pm 1$.

C. Incoherent loss processes

The nonperturbative KRS theory treats resonant capture and resonant loss self-consistently. However, resonant ionization is not the only loss process that depletes the population of a given excited manifold. Collisions between projectile electrons and target electrons in
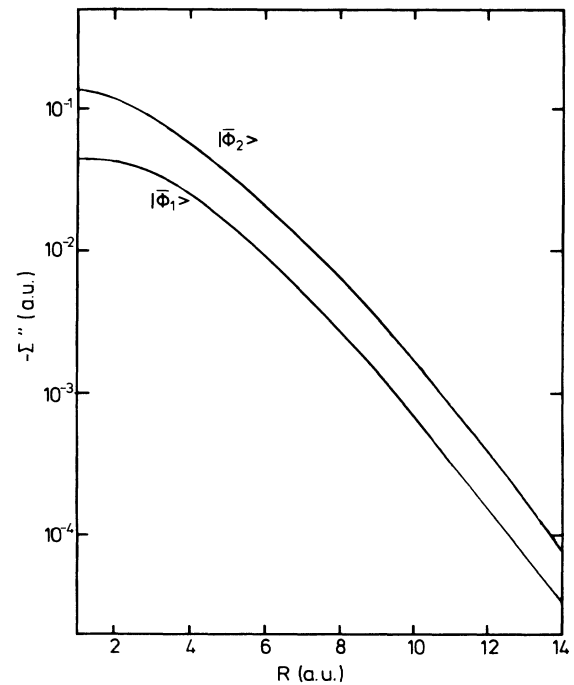
FIG. 7. Imaginary part of the self-energies, Σ''_j, as a function of the distance R from the jellium surface.
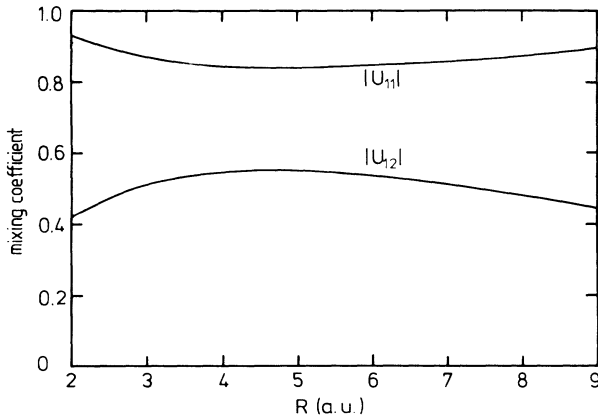
FIG. 8. Moduli of the expansion coefficients U_{11} and U_{12} of the eigenstate $\bar{\phi}_1$ of the self-energy matrix in terms of the atomic states $2s$ and $2p_0$, respectively.

the vicinity of the surface cause additional nonresonant ionization (or transitions to other n levels). A realistic description of ion-surface scattering requires the incorporation of doubly inelastic processes leading to both target and projectile excitation. Since such an excited two-electron final state is not included in the one-electron state space and is experimentally not resolved, we treat doubly inelastic scattering events as incoherent loss processes, i.e., as a sink for probability flux neglecting thereby possible effects on relative phases of scattering amplitudes. Accordingly, we add to the decay constant $(-\Sigma_j'')$ a state-independent damping term $\Gamma_I/2$,
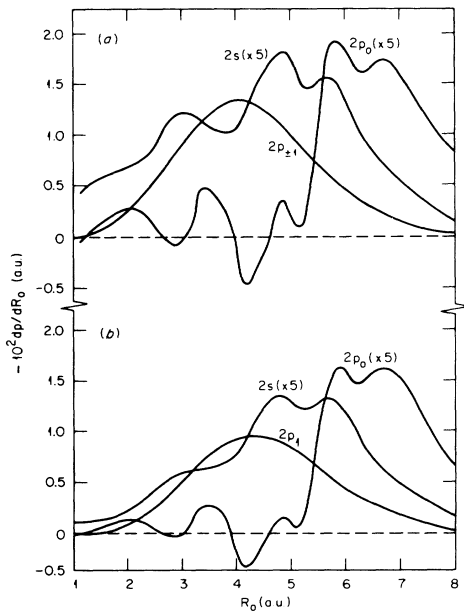
$$[-\tilde{\Sigma}_j''(R)] = [-\Sigma_j''(R)] + \Gamma_I(R)/2 , \tag{40}$$

with the damping due to the incoherent scattering given by

$$\Gamma_I = \frac{vn(R)}{\lambda_I n(0)} . \tag{41}$$

In Eq. (41), $n(R)$ and $n(0)$ denote the target electron density at the distance R from the surface and in the bulk, respectively. As a crude estimate we use the value $\lambda_I \cong 5$ a.u. for the inelastic bulk mean free path[26] λ_I for free electrons.

D. Distance of excited-state formation

The dependence of the capture probability $\rho_{2p\pm1,2p\pm1}$ as a function of the initial distance of the outward propagation, R_0, is displayed in Fig. 10. We find at small R_0 an order-of-magnitude discrepancy between the KRS theory and the first-order approximation. The nonperturbative treatment yields a characteristic saturation behavior for $R \leq 3$ a.u., i.e., ρ becomes independent of R. At small distances the continual creation and destruction of excited states leads to an excitation equilibrium. This loss of memory justifies the crude approximation for the trajectory near the point of closest approach mentioned above and the restriction of the electronic evolution to the outgoing portion of the trajectory. At large values of R_0, ρ approaches the first-order (Born) approximation results.[12] In the present case, the validity of the Born approximation for the transfer at large distances is based on the
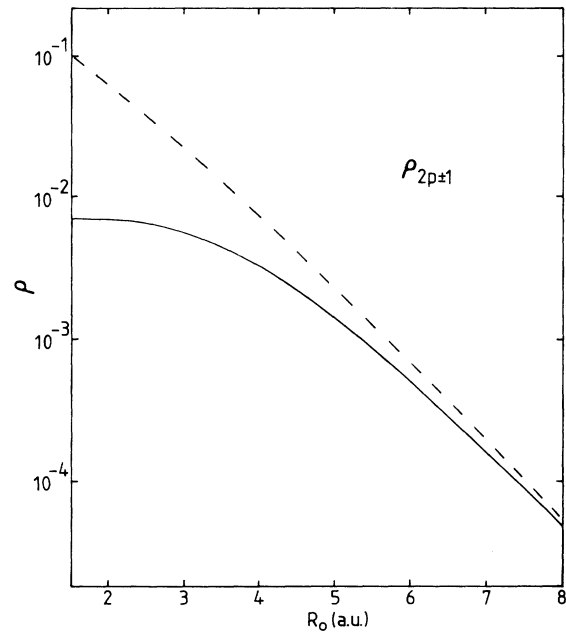

FIG. 9. Rate of change of capture probability $(-d\rho/dR_0)$ for all substates H $(2lm)$ for P$\rightarrow$Au $(v=0.7$ a.u., $\theta=5°)$ with or without incoherent loss. (a) $\Gamma_I=0$, see Eq. (40); (b) $\Gamma_I\neq0$. The surface normal is the quantization axis.

FIG. 10. Probability $\rho(R_0)$ for capture into the $2p\pm1$ state for H$^+$ + Au $(v=1, \theta=5°)$ as function of the lower limit R_0 of the outward $R(t)$ integration. The surface normal is the quantization axis. $- - -$, Born approximation; ——, present KRS theory.

weakness of the coupling rather than the high projectile speed collisions. We also note that second-order Thomas double scattering[27] is not important in this case since the planar channel potential V_f does not support a 60° scattering event back into forward direction as required for the kinematics of the Thomas process. This is not to say that other off-shell second-order contributions describing scattering into continuum intermediate states and not being included in the finite-dimensional matrix equation [Eq. (22)] are always unimportant. In fact, for collisions at high velocities involving the atomic target core and resembling more closely ion-atom collision, the Thomas process is expected to contribute significantly.

The saturation behavior of ρ due to the presence of loss processes has also important implications concerning the relative importance of nonresonant and resonant processes. While based on a first-order estimate, the nonresonant capture probability is small compared to the probability for resonant transfer; the simultaneous presence of a strong loss channel reduces the relative effectiveness of a kinetic resonance compared to nonresonant processes where the probability flux is small in both directions. The neglect of nonresonant capture processes needs therefore additional justification on a case-by-case basis. For P$\rightarrow$Au scattering at $v \cong 1$, for example, we find that the first-order nonresonant capture into the $1s$ state (without taking into account loss) is smaller than the KRS probability $\rho_{n=2}$ including loss processes. This indicates that the kinematic resonance is indeed the dominant mode of formation of neutral hydrogen H($n=2$).

The velocity dependence of ρ (Fig. 11) is displayed only over a fairly narrow range of velocities $v_F \lesssim v \lesssim 2v_F$. The rapid decay of ρ at higher v clearly indicates that capture from inner shells becomes important for $v > 1$. On the other hand, while for $v < v_F$ the present formulation is expected to provide a realistic description, its full numerical treatment poses a formidable task in view of the rapidly oscillating phase factors [Eq. (25)]. Even at intermediate velocities, the oscillating structure of the integrands limits the numerical accuracy which is estimated to be in the

area of 10%. Saddle-point approximation techniques[14,28] are probably more adequate to treat the limit $v \ll v_F$. The same is true for the limit $\theta \rightarrow 0$.

The most probable distance for the formation can be inferred from the rate of change in probability, $-d\rho/dR_0$ [Fig. 9]. Roughly, capture takes place at a distance $R \cong \langle r \rangle_{n=2}$ from the jellium surface, corresponding to distance of $R = \langle r \rangle_{n=2} + a/2$ (a is the lattice constant) from the outermost atomic layer of a real metal surface.[29] This explains the qualitative agreement with earlier Born approximation calculations[12] when a phenomenological cutoff $R_0 \geq \langle r \rangle_n$ was introduced. We note a qualitative similarity of the present $(-d\rho/dR_0)$ curve with the spatial weighting function[30] for capture derived within a fixed-ion approximation for hyperthermal surface scattering. The oscillatory structures are due to the strong $2s$-$2p_0$ mixing near the surface.

A simple physical picture emerges: At distances $R \ll \langle r \rangle_n$ the coupling of atomic levels to the unoccupied levels in the solid is so strong that the formation of excited states is followed by loss. At large distances ($R \gg \langle r \rangle_n$), the coupling is so weak that the probability flux in both directions is small despite the resonant nature of the process. The final-state formation effectively takes place in the transition region between these two regions.

The influence of incoherent loss processes is also displayed in Fig. 9. The major effect of a nonzero Γ_I [Fig. 9(b)] is an overall reduction of ρ and a slight shift of the distance of formation towards larger distances compared to calculation with $\Gamma_I = 0$ [Fig. 9(a)]. We note that coherence parameters and polarizations are only slightly affected.

The present calculation reveals a state and velocity dependence of the excited-state formation. Formation of the $2p$ ($m = \pm 1$) and the $2s$ states generally take place at smaller R than formation of the $2p_0$ state. For $v \gtrsim 1$ we find $\rho(R_0)$ to oscillate around its equilibrium value for small R_0. The onset of this effect can be already observed at $v = 0.7$. The effective distance of formation is fairly delocalized with a width $\Delta R \cong 3$–4 a.u.

E. Coherence parameters

In this section we discuss results for the complete $n=2$ density matrix.

A characteristic feature in the elliptical polarization (Fig. 12) is the strong circular polarization S/I pointing to a rotating charge cloud in agreement with the classical density gradient model.[11–12] We also find relatively large values of C/I, while first-order[12] and Anderson-model[14] calculations give $C/I = 0$. The large values for the linear polarization parameter, M/I, not observed in the experiment result from the enhanced resonant ionization probability of the $2p_0$ state (aligned along the surface normal chosen as quantization axis) relative to corresponding loss probability of the $2p \pm 1$ state (parallel to the surface plane). The polarization parameters, in particular M/I, are rather sensitive to the input data for the static ion-surface interaction (e.g., the self-energy matrix) used in the present dynamical treatment for charge exchange. The significance of the numerical values employing a
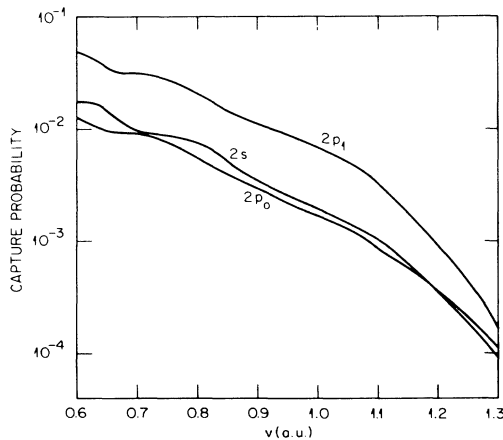
FIG. 11. Diagonal elements of the density matrix $\rho_{j,j}$ as a function of v. The surface normal is the quantization axis.
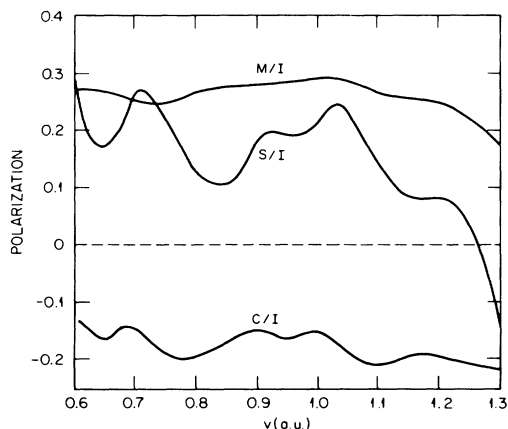
FIG. 12. Relative Stokes parameters S/I, M/I, and C/I for the doublet transition $H(2\,^2P \rightarrow 1\,^2S)$ as a function of v. M/I and C/I are defined relative to the $\hat{v}$ axis (see text).

Sommerfeld model for target structure should therefore not be overestimated. An attractive alternative for future investigations would be to employ an R-dependent phenomenological self-energy matrix as static input that reproduces the experimental (or theoretical) shift and width of energy levels of adsorbed atoms at equilibrium distances from the surface.

Combining the information on the polarization with the results for other coherence parameters (Fig. 13) a complete quasiclassical picture (Fig. 14) of the electronic orbit formed in ion-surface interation can be constructed. The values of $\langle A_x \rangle$ and $\langle A_z \rangle$ indicate that the electron is in front of the projectile and is located between the surface and the projectile. This is completely consistent with the orientation of the major axis of the elliptic polarization as defined by $M/I > 0$ and $C/I < 0$. According to S/I (proportional to $\langle -L_y \rangle$) the rotation of the electron is clockwise in accordance with the density gradient model. The results for the small coherence parameters $\langle (\mathbf{L} \times \mathbf{A}) \rangle$ can
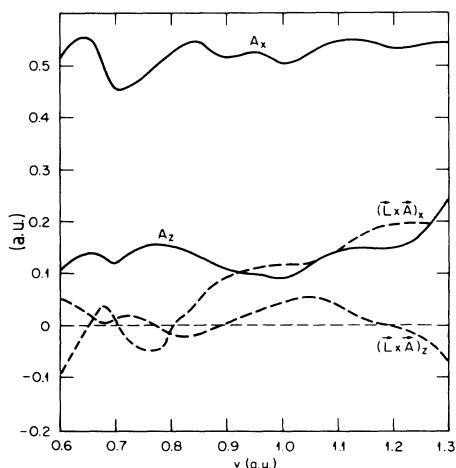

FIG. 13. Coherence parameters $\langle A_x \rangle$, $\langle A_z \rangle$, $\langle (\mathbf{L} \times \mathbf{A})_x \rangle$, and $\langle (\mathbf{L} \times \mathbf{A})_z \rangle$ as a function of v. The surface normal is the quantization axis.
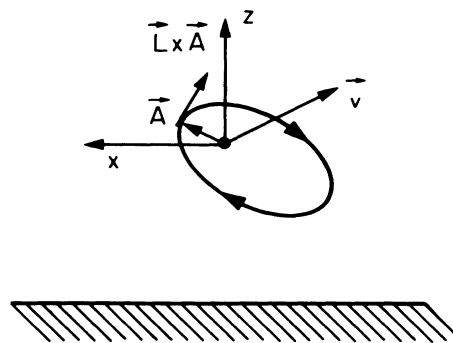

FIG. 14. Classical Kepler orbit as predicted by quantum-mechanical expectation values at $v \cong 0.82$ (schematically). Only the relative orientation of various vectors to each other is significant; their magnitude is arbitrary.

be consistently combined with $\langle L_y \rangle$ and $\langle \mathbf{A} \rangle$ to form a classical orbit at certain velocities near $v \cong 0.8$ as displayed in Fig. 14. We note that the number of statistically independent quantum-mechanical expectation values for rank-1 tensors [Eq. (33)] exceeds the number of independent classical orbital parameters for a single ellipse. The fact that the quantum-mechanical expectation values turn out to be interrelated in such a way that they can be consistently combined to a single classical orbital picture clearly indicates the physical significance of such a classical interpretation even though such a correspondence is far from being exact. The latter is underlined by the fact that the direction of the $\mathbf{L} \times \mathbf{A}$ vector cannot be accommodated within the simple picture at other velocities.

V. RELATION TO OTHER THEORIES

The present KRS theory for resonant charge transfer contains several previously suggested models as special cases. In order to make the physical content of the present formulation more transparent we briefly discuss its relation to other models.

A. Anderson-model Hamiltonian

Recently, a treatment of resonant charge transfer employing a time-dependent Anderson-model Hamiltonian has been proposed.[14,28] An essential difference to the present formulation is its single-channel character neglecting nonorthogonality connection and lacking the identification of channel potentials. In addition, the authors invoke several additional model assumptions regarding the coupling matrix elements. The latter complicates a quantitative comparison. We nevertheless can reproduce the basic Anderson-model Hamiltonian result [Eq. (8) in Ref. 14] if we apply in addition to all the approximations used in Sec. IV the following assumptions: (a) $N_j = 0$ in $\mathbf{\Sigma}$, (b) neglect of all higher-order multipoles of the image interactions in V_f beyond the R^{-1} term, (c) neglect of the principal part integral in Eq. (38) which would contain now V_i rather than V_f and would approach a nonzero value at infinity, (d) use of the diabatic instead of the adi-

abatic [Eqs. (28) and (29)] transformation, and (e) neglect of the Pauli correction in $\underline{\Sigma}$ [Eq. (39)].

B. Bassel-Gerjuoy and related approximations

Nonorthogonality corrections have been previously treated in various approximations in high-energy ion-atom collisions. A well-known example is the first-order perturbation approximation to a two-state close-coupling model suggested by Bassel and Gerjuoy.[31]

The present formulation can be reduced to the Bassel-Gerjuoy approximation in two steps: (a) If one retains the nonorthogonality correction N_j in B_j but neglects all matrix elements M_j as well as off-diagonal elements $\langle \phi_j | V_f | \phi_{j'} \rangle$ $(j \neq j')$ in $\underline{\Sigma}$, one arrives at a distorted-wave version of the Bassel-Gerjuoy approximation. (b) If one, in addition to the step (a), neglects the diagonal distortions in both the entrance channel, $\langle \phi_k | V_i | \phi_k \rangle$, and the exit channel, $\langle \phi_j | V_f | \phi_j \rangle$, the standard Bassel-Gerjuoy approximation is recovered.

C. The Born approximation

The Born approximation to charge transfer, usually referred to as the Oppenheimer-Brinkman-Kramers (OBK) approximation,[31] follows from Eq. (25) if one neglects the self-energy matrix as well as channel distortions and the orthogonalization correction altogether. The OBK approximation as well as the Bassel-Gerjuoy approximation do not account for back-coupling, i.e., loss is not treated self-consistently. This leads to unphysically large contributions from small distances. However, one can improve the approximation by introducing a cutoff[12] $R \geq \langle r \rangle_n$, in order to account for loss on a phenomenological level.

VI. CONCLUDING REMARKS

We have presented a nonperturbative theory for resonant charge transfer at intermediate distance through a kinematic resonance. It treats resonant capture and resonant loss self-consistently. The multichannel nature of the process manifests itself in the influence of nonorthogonality corrections and in the presence of different channel potentials which play an important role. In particular, the energy shift of an atomic level near a jellium surface described by a semi-infinite Sommerfeld electron gas approaches the correct asymptotic value of the free atom only if nonorthogonality corrections are taken into account. The numerical results for electron pickup into the substates of the $n = 2$ manifold in proton-gold surface collisions show that the formation of excited states preferentially takes place at intermediate distances $R \cong \langle r \rangle_n$ from the jellium surface. From an analysis of the complete $H(n = 2)$ density matrix the following picture of the charge cloud asymmetry emerges: The center of gravity of the electronic charge cloud is in front of the receding proton and is located between the proton and the surface. The sense of circulation is in accordance with the classical density gradient model.[11,12]

While quantitatively different from earlier Born approximation calculations,[12] many qualitative features have been confirmed. Additional effects beyond the resonant charge exchange, such as electron loss due to doubly inelastic processes, are found to give non-negligible contributions.

Several limitations of the present model are worth mentioning and point to avenues of further developments: In the present investigation we have focused on resonant transitions between bound states (tunneling or subbarrier processes). At small distances from the surface projectile states can become unbound due to the surface interaction leading to classically allowed "over the barrier" transitions. The influence of those processes is presently under investigation. At high collision velocities $v > 1$ a.u., broadened resonances with localized inner-shell levels of the target not yet taken into account become important. At low velocities $v \ll v_F$, saddle-point approximation techniques should be implemented in order to investigate the approach of the static limit and its relation to the fixed-ion approximation since the full numerical treatment becomes unworkable in this region. For highly charged ions with many excited states in (static) resonance with the occupied conduction band, the relative motion mediating kinematic resonances ceases to be of crucial importance for the transfer. In this case, the large amount of well-localized potential energy rather than the kinetic energy induces inelastic processes. Finally, the present treatment is restricted to the independent-particle model. The formation of H^- in grazing-incidence scattering of protons[6] pointing to the possibility of correlated two-electron processes requires a study of correlated two-electron wave function in an ion-surface potential.

The picture of a kinematic resonance (Fig. 1) also implies the possibility of forming highly excited Rydberg states $(n \rightarrow \infty)$ and near-threshold continuum states. For sufficiently high v $(\cong v_F)$ the Galilei-shifted band structure overlaps with the threshold region. This would allow resonant capture into low-lying continuum states of the projectile. The recently observed electron spectra[32–34] display a broad peak near the projectile velocity with anisotropic structures[34] due to the low symmetry of ion-surface interaction.

APPENDIX A

In this appendix, we show that the distortion in Eq. (19) is negligible for completely delocalized Sommerfeld wave functions for the conduction band for a semi-infinite electron gas, i.e.,

$$\lim_{\mathscr{V} \to \infty} \langle \phi_k | V_i | \phi_k \rangle \rightarrow 0 , \tag{A1}$$

where $\mathscr{V}$ is the periodicity volume. We note first that the channel potential V_i [Eq. (7)] is well defined only for coordinates outside the surface. Inside the solid we may assume perfect screening. According to Eq. (10) the matrix element (A1) is of the form

$$\langle \phi_{\mathbf{k}} | V_i | \phi_{\mathbf{k}} \rangle = \frac{1}{\mathscr{V}} \frac{4k_z^2}{k_z^2 + \delta^2} \int_{z>0} d^3 r \, e^{-2\delta z} \left[-\frac{1}{[x^2+y^2+(R-z)^2]^{1/2}} + \frac{1}{[x^2+y^2+(z+R)^2]^{1/2}} - \frac{1}{[x^2+y^2+(2z)^2]^{1/2}} \right] ,$$

$$(A2)$$

where we have here chosen the origin of the coordinate system to coincide with the jellium surface deviating from the original choice [see Eqs. (1) and (2) and Appendix B]. It is sufficient to discuss the first term of (A2) since the others can be treated analogously. Introducing cylindrical coordinates we get

$$-\frac{\pi}{\mathscr{V}} \frac{4k_z^2}{k_z^2 + \delta^2} \int_0^\infty dz \int_0^{b_0^2} db^2 e^{-2\delta z} \frac{1}{[b^2+(R-z)^2]^{1/2}}$$

$$(A3)$$

where b_0 is of the order of $\mathscr{V}^{1/3}$. Performing the b integral we find for finite b_0

$$-\frac{\pi}{\mathscr{V}} \frac{8k_z^2}{k_z^2 + \delta^2} \int_0^\infty dz \, e^{-2\delta z} \{ [b_0^2+(R-z)^2]^{1/2} - |R-z| \}.$$

$$(A4)$$

For all bound states of the metal with δ real and positive the z integral converges and is for large but finite $b_0(b_0 \gg R)$ of the form

$$-\frac{\pi}{\mathscr{V}} \frac{8k_z^2}{k_z^2 + \delta^2} \, (\text{const} b_0 - \text{const}') .$$

$$(A5)$$

In the limit $\mathscr{V} \to \infty$ and $b_0 \propto \mathscr{V}^{1/3}$ the first term behaves like $\mathscr{V}^{-2/3}$ while the second goes like $\mathscr{V}^{-1}$. The distortion is therefore negligible for conduction-band states.

APPENDIX B

Adopting a coordinate frame with the proton at the origin the total image potential felt by the electron is given by

$$V^{\text{image}} = V_C^I + V_e^I$$

$$= \frac{q}{[x^2+y^2+(z+2R)^2]^{1/2}} - \frac{1}{4(z+R)} , \quad (B1)$$

where q is the charge of the ion prior to capture and $z \geq -R$. A straightforward multipole expansion leads to

$$V^{\text{image}} = \frac{1}{2R}(q - \tfrac{1}{2}) - \frac{z}{4R^2}(q-1)$$

$$+ \frac{1}{4R^3} \left[(q-2/3)\frac{3z^2-r^2}{2} - \tfrac{1}{3}r^2 \right] + O(R^{-4}) .$$

$$(B2)$$

Note that the monopole term $(\sim R^{-1})$ is nonzero even for singly charged ions which together with the electron form a neutral atom. This is due to the fact that the corresponding interactions of the ion with the image charges are not included in the potential energy in the *electronic* Hamiltonian [Eqs. (3) and (B1)]. On the other hand, the dipole term $(\sim R^{-2})$ vanishes for neutral atoms $(q=1)$. In this case, the term R^{-3} induces static state-dependent splittings to lowest order. For brevity we will refer to the latter as the quadrupolar term even though it also includes a scalar contribution. We note that the multipole approximation breaks down for small $R \ll \langle r \rangle$ compared to the radius of the excited projectile state.

ACKNOWLEDGMENT

[1]H. J. Andrä, Phys. Lett. **54A**, 315 (1975).

[2]H. G. Berry, G. Gabrielse, A. E. Livingston, R. M. Schectman, and J. Desesquelles, Phys. Rev. Lett. **38**, 1473 (1977).

[3]N. Tolk, J. C. Tully, J. S. Kraus, W. Heiland, and S. H. Neff, Phys. Rev. Lett. **41**, 643 (1978).

[4]H. Winter and R. Zimny, Hyperfine Interactions **22**, 237 (1985).

[5]W. Graser and C. Varelas, in *Inelastic Particle-Surface Collisions*, Vol. 17 of *Springer Series in Chemical Physics*, edited by E. Taglauer and W. Heiland (Springer, Berlin, 1981), p. 211.

[6]C. Rau, J. Magn. Mater. **30**, 141 (1982).

[7]S. S. Shekther, Zh. Eksp. Teor. Fiz. **7**, 750 (1937).

[8]B. A. Trubnikov and Y. N. Yavlinskii, Zh. Eksp. Teor. Fiz. **52**, 1638 (1967) [Sov. Phys.—JETP **25**, 1089 (1967)].

[9]R. K. Janev, J. Phys. B **7**, 1506 (1974).

[10]H. J. Andrä, R. Zimny, H. Winter, and H. Hagedorn, Nucl. Inst. Methods B **9**, 572 (1985).

[11]H. Schröder and E. Kupfer, Z. Phys. A **279**, 13 (1976).

[12]J. Burgdörfer, H. Gabriel, and H. Schröder, Z. Phys. A **295**, 7 (1980); H. Schröder and J. Burgdörfer, in *Inelastic Particle-Surface Collisions*, Ref. 5, p. 207.

[13]J. van Wunnik, R. Brako, K. Makoshi, and D. Newns, Surf. Sci. **126**, 618 (1983).

[14]R. Brako, Phys. Rev. B **30**, 5629 (1984).

[15]J. W. Gadzuk, Surf. Sci. **6**, 133 (1967).

[16]H. Schröder, Nucl. Instrum. Methods B **2**, 213 (1984).

[17]R. Ray and G. D. Mahan, Phys. Lett. **42A**, 301 (1972); J. Muscat and D. M. Newns, Surf. Sci. **64**, 641 (1977).

[18]H. C. Brinkman and H. A. Kramers, Proc. R. Acad. Sci. (Amsterdam) **33**, 973 (1930).

[19]I. Lindgren and J. Morrison, *Atomic Many Body Theory* (Springer-Verlag, Berlin, 1982).

[20]H. Schröder, Z. Phys. A **284**, 125 (1978).

[21]See, e.g., H. J. Andrä, Phys. Scr. **9**, 257 (1974).

[22]J. Burgdörfer, Z. Phys. A **309**, 285 (1983).

[23]J. Burgdörfer, Ph.D. thesis, Freie Universität Berlin, 1981 (unpublished).

[24]T. G. Eck, Phys. Rev. Lett. **31**, 270 (1973); see also I. Sellin, J. Mowat, R. S. Peterson, P. M. Griffin, R. Laubert, and H. Haselton, *ibid*. **31**, 1335 (1973); A. Gaupp, H. J. Andrä, and J. Macek, *ibid*. **32**, 268 (1974).

[25]See, e.g., W. Louisell, *Radiation and Noise in Quantum Elec-*

tronics (McGraw-Hill, New York, 1964), Chap. 5.

[26]C. Tung, J. Ashley, and R. Ritchie, Surf. Sci. **81**, 409 (1979).

[27]R. Shakeshaft and L. Spruch, Rev. Mod. Phys. **51**, 369 (1979).

[28]D. M. Newns, K. Makoshi, R. Brako, and J. N. M. van Wunnik, Phys. Scr. **T6**, 3 (1983).

[29]T. P. Grozdanov and R. K. Janev, Phys. Lett. A **65**, 396 (1978).

[30]E. G. Overbosch, B. Rasser, A. D. Tenner, and J. Los, Surf. Sci. **92**, 310 (1980).

[31]See, e.g., M. R. C. McDowell and J. P. Coleman, *Introduction to the Theory of Ion-Atom Collisions* (North-Holland, Amsterdam, 1970), Chap. 4.

[32]For a review see M. Breinig *et al.*, Phys. Rev. A **25**, 3015 (1982); K. Groeneveld, W. Meckbach, I. Sellin, and J. Burgdörfer, Comments At. Mol. Phys. **14**, 187 (1984).

[33]L. F. de Ferrariis and R. A. Baragiola, Phys. Rev. A **36**, 4449 (1986).

[34]H. Winter (private communication).